Desalination 586 (2024) 117869

Contents lists available at ScienceDirect

Desalination

journal homepage: www.elsevier.com/locate/desal

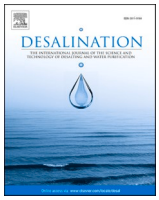

Understanding interfacial polymerization in the formation of polyamide RO membranes by molecular simulations

Gan Liu [a], Mingjie Wei [a,*], Daiwen Li [a], Ming Liu [a], Jun Huang [a], Yong Wang [a,b]

[a] State Key Laboratory of Materials-Oriented Chemical Engineering, College of Chemical Engineering, Nanjing Tech University, Nanjing 211816, Jiangsu, China
[b] School of Energy and Environment, Southeast University, Nanjing 210096, Jiangsu, China

HIGHLIGHTS

- Atomic modelling of crosslinked polyamide membranes at the dual-solvent interface
- Molecular structures changes at various stages of interfacial polymerization.
- Investigation on monomer diffusion and its impact on the subsequent reactions
- Promotion of TMC concentration yields thicker membranes with dropped permeance.

GRAPHICAL ABSTRACT

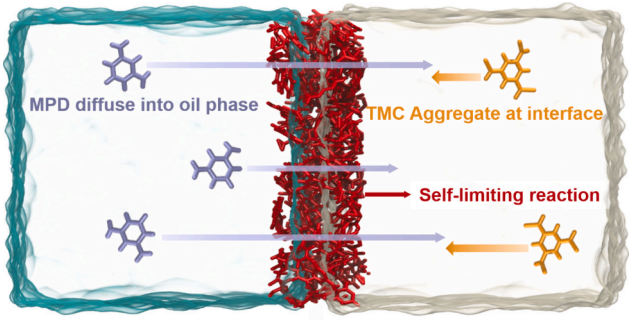

Depth of MPD diffusion determines membrane thickness.

ARTICLE INFO

Keywords:
Polyamide
Reverse osmosis
Molecular dynamics
Polymerization mechanism
Solvents

ABSTRACT

Since the water permeation mechanisms of polyamide membranes are highly dependent on the micro-structure of polyamide membranes, a deeper understanding of the formation process of them is necessary for the optimization of the membrane performance. As most simulation works construct the polyamide membranes in an ideal way, the interfacial diffusion of monomers, which is crucial for the formation of polyamide membranes, is usually ignored. To address this issue, we mimic the experimental conditions to develop an atomic model of a highly crosslinked polyamide membrane by conducting molecular dynamics simulations. Via tuning the concentration and molar ratio of monomers, the diffusion of monomers and its influence on the subsequent reaction are altered, and the final membrane structure consequently changed. Simulation results reveal that increasing the trimesoyl chloride concentration results in thicker membranes with a reduced specific surface area and consequently decreased water permeance. On the other hand, increasing the *m*-phenylenediamine concentration will accelerate the reaction rate and reduce the final crosslinking degree. A deeper understanding of the mechanism of polyamide-membrane formation is unveiled in this work, which can aid in the design of high-performance polyamide membranes in the future.

* Corresponding author.
E-mail address: mj.wei@njtech.edu.cn (M. Wei).

https://doi.org/10.1016/j.desal.2024.117869
Received 16 April 2024; Received in revised form 20 June 2024; Accepted 22 June 2024
Available online 24 June 2024

1. Introduction

Due to the rapid global population growth, the scarcity of freshwater resources has become a pressing issue, with approximately one-third of the world's population already facing water shortage [1]. To address this, the most promising solution is the use of desalination technologies to extract freshwater from seawater [2]. The use of reverse osmosis (RO) technology has become increasingly popular in the current market for the purpose of obtaining fresh water from seawater or wastewater. RO membranes, as the core of this technology, directly determine the RO performance, including salt rejection and water permeance [3,4]. The salt rejection rate of RO membranes available on the market is usually more than 99 %, meeting the requirements of freshwater. However, the water permeance of RO is not satisfactory due to the rapidly-increasing demand of freshwater. As a result, researchers are actively exploring ways to develop high-permeance RO membranes without sacrificing the ion rejection, as enhanced water–solute selectivity rather than enhanced water permeability has impact on the efficiency of desalination processes [5]. The current RO membrane is mainly composed of three layers, namely highly-cross-linked aromatic polyamide (PA) selective layer, polysulfone support layer, and non-woven fabric layers. The PA layer plays a significant role in separation and is the main source of transport resistance of water molecules, therefore, the permeability of such layer is mostly focused by researchers [6,7].

The most proposed strategy of promoting the permeance of PA layer is reducing its thickness [8], which is proportional to the transport resistance [9,10]. Besides, preparing mixed-matrix PA membranes is an alternative strategy. By incorporating nanoparticles into PA membranes, the permeability is evidently promoted [11–13]. In order to further promote the permeability of PA layers, it is essential to figure out the permeance mechanism of water molecules through them from the microscopic level.

Molecular dynamics (MD) simulation, which is a powerful tool to observe the molecular motion, is usually applied to investigate the transport mechanism of PA RO membranes [14–16]. The influence of pressure drops and crosslinking degrees on the permeance of pure water through PA membranes has been investigated by He et al. [17]. Our group also investigated the influence of hydrophilicity on the permeability based on the analysis of transport resistance [18]. The transport mechanism of mixed-matrix membranes was further investigated [19] and several mechanisms of permeability promotion were proposed [20–23]. Furthermore, the anti-fouling ability of PA membranes was also investigated by MD simulations [24,25].

However, the above simulations also reveal that the water permeance is highly dependent on the microscopic structure of PA. Therefore, the construction mechanism of the membrane is emergently desired before figuring out the approach of promoting permeability of PA layer. Recently, various methods have been proposed for constructing PA membranes [17]. Ding et al. [26] utilized MD simulations to randomly add a certain number of MPD into a simulation box containing multiple PA linear chains. After undergoing a period of simulation, a manual polymer crosslinking process was carried out. Harder et al. [27] used the "de novo crosslinking" dynamic polymerization method to establish the molecular model of the PA film, where trimesoyl chloride (TMC) and *m*-phenylenediamine (MPD) molecules were randomly placed into a cubic simulation box. When two monomer molecules were in proximity, they were considered to have reached the reaction conditions, and an amide bond was formed between them to replace the original acyl chloride group and amino group. Based on these methods, Freger et al. [28] improved the construction method of the PA membranes by replacing the cubic box with a rectangular simulation box that takes into account the two-dimensional nature of the membrane, and by adopting different polymerization standards at different reaction stages. Vickers et al. [29] also followed the approach of Harder et al. but dispersed TMC and MPD in n-hexane molecules for crosslinking to make the simulation more comparable to experiments. These works succeeded in constructing the highly crosslinked PA membranes for further investigation.

On the other hand, the operational conditions of interfacial polymerization (IP), e.g. the concentrations of monomers, are mostly concerned for experimental researchers, as they usually determine the performance of prepared membranes via inducing the distinct microstructures. The much excessive MPD (MPD/TMC molar ratio ranging from 4:1 to 100:1) was usually applied in experiments as the experimental researchers believed that the excessive MPD would enhance the diffusion of MPD and consequently help for the interfacial polymerization [30]. By the technique of electrospray, Chowdhury et al., prepared the ultra-thin PA membranes but at the MPD/TMC molar ratio as low as 4:1 [31]. Therefore, the diffusion of monomers, especially the interfacial one, will significantly influence the micro-structure of PA membranes as well as their permeance and desalination performance.

Summarizing the above MD simulation work, it is found that the PA membrane models were mostly constructed in a vacuum or single solvent, disregarding the impact of two immiscible solvents and their interface on the diffusion of the two monomers. Consequently, the built PA membranes are somehow idealized compared to the experimental ones. In order to unravel the interfacial polymerization for PA membrane formation, the simulation of interfacial polymerization process on PA in dual-solvent conditions is urgent to be built up.

In practical experiments, the formation of the PA RO membrane occurs at the interface of the aqueous and oil phases through the free diffusion of MPD and TMC dispersed in their respective solvents [32–34]. To accurately observe the reaction process, we employed the dual-phase interfacial polymerization (IP) simulation method, which mimics the experimental procedure. Two types of solvents, water and n-hexane, are constructed, with MPD and TMC dissolved in each solvent, respectively. Once one TMC contact a MPD, the reaction between them will occur by forming amide bond between the groups of -COCl and -NH2 from TMC and MPD, respectively. By analyzing the changes in crosslinking degree over reaction time, the relationship of membrane formation with concentration and molar ratio of monomers is revealed. The key of preparing the ultrathin PA membranes can also be uncovered in this work.

2. Simulation details

2.1. Construction of PA membranes in solvent environment

Commercial reverse osmosis (RO) membranes are commonly synthesized by IP of TMC and MPD [35]. However, due to the highly crosslinked molecular structure of the resulting PA selective layer, its accurate molecular structure is not easy to be observed directly through experimental characterizations. Therefore, a molecular simulation method was employed to establish molecular configuration and the reaction process of IP was monitored as well.

The initial molecular structure of each case was constructed by software of moltemplate [36], in which all molecules of monomers were kept as its own molecular structure, rather than the simplified monomers which were employed in most published work of PA formation in vacuum condition [9,37]. In most experiments, it is common to use a 2 wt% MPD concentration and a 0.2 wt% TMC concentration for IP reaction. Therefore, for the sake of consistency and comparability, our primary focus was on the results obtained with a 2 wt% MPD concentration. However, the concentrations of TMC are based on the specific molar ratios, which is listed in Table 1.

The monomers were randomly filled separately into two solutions according to the concentrations listed in Table 1, resulting in two parts: (1) the oil phase containing TMC and n-hexane; (2) the aqueous phase containing MPD and water. Graphene plates were placed at both ends of simulation box in the Z direction, and a pressure of 1 bar, toward to the center of simulation box, was applied onto them. Hence, two solution parts contacted together due to the existence of pressure on graphene

Table 1
The molar ratios, concentrations, and the number of monomers in the simulation for the various cases.

Case Name	Molar Ratio	Concentration (wt%)		Monomer Number	
		MPD	TMC	MPD	TMC
2 % 6:1	6:1	2.26	1.54	12	2
2 % 3:1	3:1	2.26	3.08	12	4
2 % 3:2	3:2	2.26	6.18	12	8
10 % 6:1	6:1	10.00	6.18	51	8
10 % 3:1	3:1	10.00	13.14	51	17
10 % 3:2	3:2	10.00	26.24	51	34

plates. After that, an NVT ensemble at 300 K for 1 ns was then carried out to ensure the stability and rationality of the configuration. Finally, the initial configuration for further IP reaction was established.

During the IP reaction process, all molecules, except graphene plates, could move freely in the simulation box. We designated the carbon atom of the acyl chloride group in TMC and the nitrogen atom of the amino group in MPD as specific atoms for reaction. Once the distance between these two types of atoms was less than 0.35 nm, a new amide bond was generated [38,39], followed by the chlorine atom in that group of TMC and the corresponding hydrogen atom in that group of MPD being removed. The energy was then minimized for structural accuracy and system stability. If no pair of bonding atoms was detected, an NVT ensemble at 300 K for 0.06 ns was then carried out, and the above steps were repeated several times. If no bonding was detected beyond 2 ns, the reaction was considered as terminated, then the crosslinking structures suitable for subsequent treatment process were obtained.

Since the bonding process would significantly reduce the concentration of monomers in two kinds of solution, it was necessary to supplement monomers after each bonding check step. The additional monomers were introduced into the vacuum space located between the solution and the graphene plates. The number of monomer supplementation was determined by the solution concentration, which was kept as the initial one before reaction occurred. By this approach, the concentrations of TMC and MPD in each solution were consistently maintained. The snapshots generated during the simulation run are depicted in Fig. 1.

2.2. Subsequent treatment process of crosslinking structures

After the above steps, the crosslinking structures were obtained with the existence of water, n-hexane and unreacted monomer molecules, as well as some oligomers. In experiments, the curing and washing of crosslinking structures after IP are always required to obtain the final membrane. To simulate this process, we followed the experimental method and carried out the following steps: (1) we removed the solvent molecules together with the unreacted monomers in the solvent, but retained the monomer molecules and oligomers adsorbed on the crosslinking structures; (2) we raised the reaction temperature up to 350 K. The higher temperature promoted the thermal motion of atoms and consequently increased the opportunity for specific groups to contact and react. Like the experimental one, such 'curing' would further promotes the compactness of crosslinking structures. Since it was easier for the reaction to occur at higher temperature, the time threshold for detection the pair of bonding atoms was set to 0.01 ns.

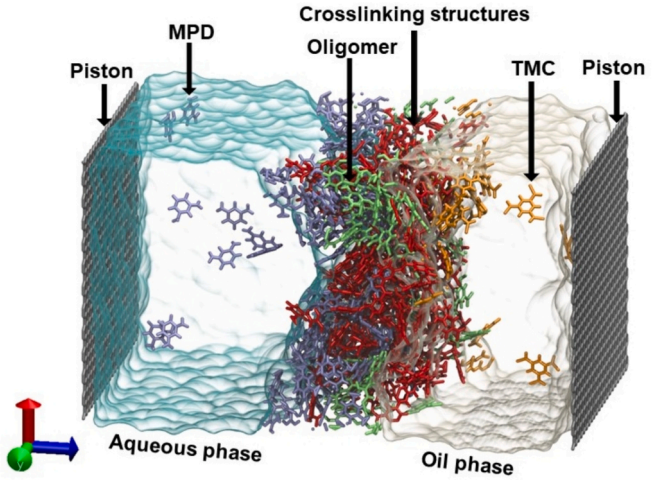

Fig. 1. The snapshot simulated IP reaction. The constituents of the simulation system have been denoted.

After that, oligomers with atom numbers less than 200 were all removed to simulate the washing process in experiments. Such a step also ensured that the membrane would not be damaged in high-pressure water flow, as small oligomers existing in PA membranes would be flushed away during the permeance test simulations. Finally, we performed the artificial hydrolysis procedure to replace all unreacted acyl chloride groups with carboxyl groups.

Six cases, listed in Table 1, were selected with various concentrations and molar ratios, and the case names will be abbreviated according to Table 1. The simulation for each case was performed itself without additional artificial intervention. When the simulation was accomplished, we got a loose dry model of PA. Afterward, the dry PA membranes were hydrated by inserting water molecules into them to expedite the hydration process, as well as placing two water reservoirs next to their surfaces. In order to push the water molecules into dry PA films, two movable graphene plates were added outside the water reservoirs as piston plates, and an external force, equivalent to1 bar, was applied on each atom of the two piston plates. We conducted a 10 ns equilibration MD simulation to ensure an adequate number of water molecules had entered the membrane, and the system had reached a stable state at the end of simulations. The hydrated PA membranes were ready for permeance and ion rejection test in non-equilibrium molecular dynamics (NEMD) simulations.

2.3. Molecular interactions and other simulation details

All simulations, including those of simulated IP, curing and membrane hydration, were performed using the Large-scale Atomic/Molecular Massively Parallel Simulator (LAMMPS) package [40]. The General Amber Force Field 2 (GAFF2) [41], which is widely adopted by many researchers for similar simulations, was used for the n-hexane, TMC and MPD. The partial charge values for each atom were obtained from the work of Gu et al. [24]. The standard SPC/E [42] model was employed for water molecules. To reduce high-frequency vibrations and simulation time, the SHAKE algorithm was used to constrain the bonds and angles of the water molecules. The Lorentz-Berthelot mixing rule was applied to all pair-wise Lennard-Jones terms, and the cut-off distances of the Lennard-Jones potentials were set to 1.5 nm. In order to reduce the influence of graphene plates on IP, the ε value of atoms in graphene plates with all other atoms was reduced to 1 % of original those, and the cut-off was set to 1.0 nm. Coulombic interactions were calculated using the particle-particle particle-mesh method (PPPM).

Three-dimensional periodic boundary conditions (PBC) were applied. The motion equation of particles was calculated using the leap-frog algorithm, with a time step of 1 fs. A Nose-Hoover style thermostat or barostat was used to maintain temperature and pressure, respectively. The canonical ensemble (NVT) was employed in most simulations including the reaction one [43]. The dimensions of the simulation box were $L_x = L_y = 5.1$ nm. Since molecules needed to be added in the Z direction, the size of the box was set large enough to avoid the interactions between the graphene plates.

The methods of NEMD simulations were similar to our previous work [44], one water reservoir with Na^+ and Cl^- ions was placed at the left side of hydrated PA membranes acting as feed side, and a pure water

reservoir was placed at right side acting the permeance side. We generated a pressure drop (ΔP) across the membrane by applying external forces to water molecules within a selected 1 nm-wide region. The external forces were applied along the Z-axis and were determined using the formula $f = \Delta PA/n$, where A is the cross-sectional area of the membrane, and n is the total number of water molecules in the chosen region. The selected ΔP value for the NEMD simulations was set at 300 MPa, significantly higher than experimental values. This deliberate choice of a high ΔP was made to maintain a high signal-to-noise ratio, which is a common practice for controlling simulation time within reasonable scales. The system's temperature was held constant at 300 K. Temperature calculations were adjusted by subtracting the center-of-mass velocity of water molecules. The NEMD simulations ran for a total of 40 ns, employing a time step of 1 fs. The initial 10 ns allowed the simulation to reach a steady state, while the remaining 30 ns were reserved for further analysis. The analysis of various membrane parameters and performance is included in the supplementary material.

3. Results and discussions

3.1. Performance of obtained PA membranes

Since the permeance and rejection performance of PA membranes are the most concerns for every researcher of RO membrane, we measure the permeance of our obtained PA membranes, which are plotted in Fig. 2a. For those six various cases, the permeance ranges from 9.38 to 200.79 L/(m^2 h bar) (LMHB). For the studies of RO membrane, there's a common standpoint that water permeance is directly related to membrane thickness. To understand the distinct permeance in wide range, we calculate the average membrane thicknesses for each case, which are shown in Fig. 2b. By comparing Fig. 2a and Fig. 2b, there is a common rule that thicker membranes have lower permeance as expected. However, the range of thicknesses locates from 1.7 to 3.2 nm. Such range cannot support the large gap of permeance. It is necessary to analyze the molecular details of each membrane.

From the experimental characterization of PA-membrane surfaces, they are hardly uniformly flat. Therefore, the average thickness cannot represent the molecular structure of PA membranes. Then, we conduct an analysis of thickness distribution in this research. Fig. 3 reveals that the 2 % 6:1 case and the 10 % 3:2 case shared a common characteristic in terms of thickness. Both cases exhibited relatively thin regions (blue) within the membrane and the thickness even drops to zero in some areas. This suggests that structural damage is responsible for the considerable increase in permeance for these two cases. The reduced rejection (around 60 %) to NaCl of these membranes could also support for this damage as other membranes exhibit NaCl rejections as high as 100 %, indicating their integrated and damage-free structure. If we carefully compare the permeance and average thickness results, it is found that the 2 % 3:1 case has thinner thickness with 10 % 3:1 case, but its permeance is much lower than the one of 10 % 3:1. It implies that more structural details should be revealed. As suggested by Culp et al. [45] and McCutcheon et al. [46], the PA density rather than thickness are the most important factor for determining the water permeance of PA RO membranes. Hence, we also plot the XY-plane maps of density for all membranes in Fig. S1. It is evident that the density distributions are similar to those of thickness. The membrane damage can also be found in the cases of 2 % 6:1 and 10 % 3:2.

We then turn to measure the membrane's porosity and specific surface area. As shown in Fig. 4, the trend of these two measurements exhibits a high degree of similarity, where high-permeance membranes had greater specific surface areas and porosities. Larger specific surface area and higher porosity indicate that there will be more surface area available for the contact of water molecules if the mass of membranes is the same.

From the above discussions, the distinct reaction conditions, e.g., molar ratio and monomer concentration, have a significant impact on the structure of PA membranes. Since the molecular structure of PA membranes results from the IP reactions, we will focus on how the IP reaction process affects the final membrane structure in the discussion below. Given that the construction of PA membranes involves two distinct processes, IP reaction and subsequent post-treatment process, we will discuss them separately.

3.2. The diffusion process of monomers in solvents

Since the reaction between two types of monomers occurs very rapidly, the current methods for synthesizing PA membranes are adjusting liquid-phase reactions primarily by controlling the diffusion of monomers. Therefore, we firstly investigate the diffusion performance of the two monomers, TMC and MPD in n-hexane and water, respectively. By performing equilibrium MD simulations, the self-diffusion coefficient of TMC in n-hexane is found to be 1.27×10^{-9} m^2/s, while MPD in water has a self-diffusion coefficient of 1.09×10^{-9} m^2/s. This confirms that TMC diffuses more rapidly in the oil phase compared to MPD in the aqueous phase.

It is generally considered that the IP reactions occur at the side of oil phase with MPD diffusing from aqueous to the oil phase. Thus, MPD must overcome diffusion resistance not only in the oil phase but also at the aqueous-oil interface. Together with the lower self-diffusion coefficient, there is a significant concentration distinction between the MPD and the TMC in experimental IP processes. In most experiments, the calculated molar ratio is usually much larger than the stoichiometric ratio of 3:2. Karan et al. proposed that they could use lower MPD concentrations to obtain PA membranes with a thickness below 10 nm [47]. Such phenomenon indicates that lowering MPD concentration (or molar ratio) can effectively reduce PA membrane thickness and consequently enhance its permeance. However, that article does not clarify the impact of diffusion on membrane performance due to the limitations of experimental methods. We believe that all adjustments to the conditions of the IP process are microscopically influencing the diffusion process of

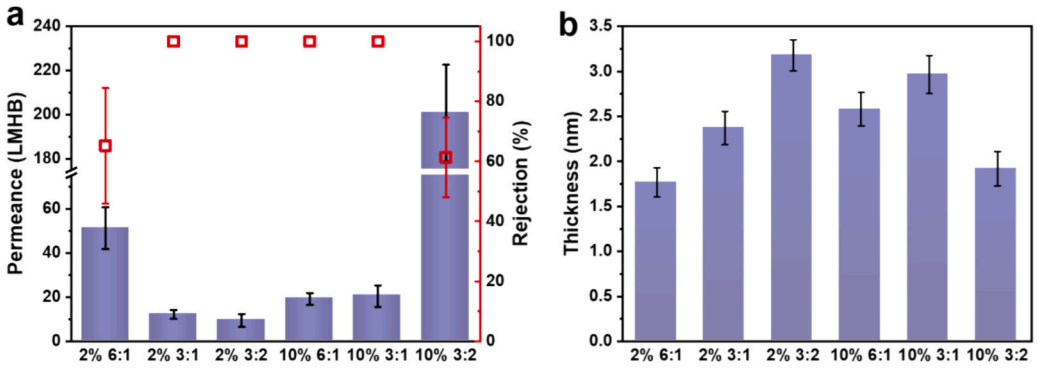

Fig. 2. Pure water permeance with rejection to NaCl (a) and the thickness (b) of all membranes.

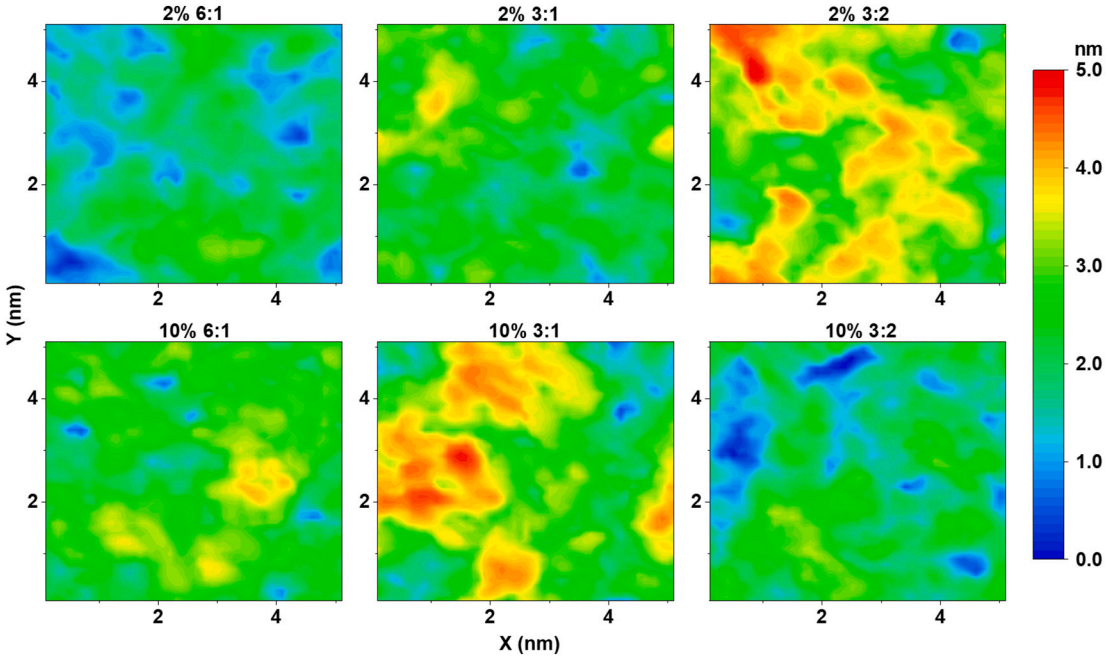

Fig. 3. The XY-plane maps of thickness for all membranes.

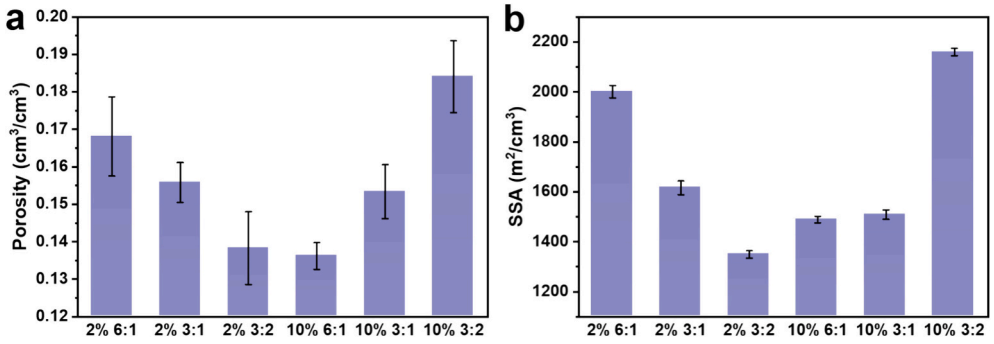

Fig. 4. The porosity (a) and specific surface area (b) of all membranes.

monomers. Therefore, it is crucial to investigate the diffusion process during the IP process to understand its influence on membrane performance.

A non-reactive diffusion-only model is then performed. In this model, 12 MPD molecules were randomly dispersed in the aqueous solvent, while 8 TMC were randomly distributed in the oil phase solvent, then an equilibrium MD simulation is carried out.

During the initial stage of the simulation (0.2 ns), TMC diffuse to the interface and remain there, while MPD manages to cross the interface into the oil phase and contact with TMC. Some MPD molecules stay at the interface due to the presence of TMC, while others continue to diffuse deeper into the oil phase. After that, MPD molecules that have penetrated deeper into the oil phase gradually return to the interface because they are attracted by the accumulation of TMC near the interface (3 ns). Ultimately, both types of monomers predominantly gathered at the interface, leaning toward the oil phase (6 ns).

The non-reactive diffusion-only simulation demonstrates that the IP process involves the diffusion of MPD into n-hexane and its subsequent reaction with the TMC at interface, resulting in the formation of a crosslinking structure. It can be concluded that the IP reaction occurs on the oil-phase side of the interface region, rather than both sides of the interface.

For the cases of 2 % concentration, the risen molar ratio (6,1) will lead to a large amount of MPD diffusing into oil phase and reach a deep position in oil position. However, they will diffuse back to the interfacial region due to its interaction with TMC, which has already accumulated at the interfacial region (shown in Fig. S2a). Such phenomenon also occurs when the concentration reaches to 10 %. However, the diffusion back of MPD to the interfacial region are restricted due to the extremely large amount of them near there (shown in Fig. S2c).

If we compare the diffusion results between various molar ratios and concentrations, it is evidently that the final state of all non-reaction diffusion looks similar. Only non-reaction diffusion procedure cannot illustrate the variation of microscopic details of membranes. The investigation of coupling of reaction and diffusion is needed.

3.3. Process of IP reactions in solvent environment

3.3.1. Various stages of IP process

After performing the non-reactive model, we then turn to the reaction process. Firstly, the density distributions of monomers, oligomers, and crosslinking structures along the normal direction of interface are calculated (shown in Fig. 6). It should be mentioned that the oligomers are defined as the post-reaction molecules with atom number less than 200, while the crosslinking structures are those with larger atom numbers. Taking the case of 2 % 3:2 as example, four various stages of IP

process, 1/4, 1/2, 3/4 and the end of reaction, are selected. It is evident that the density of crosslinking structure is promoted with the progression of the reaction. This increase will certainly slow down the mobility of monomers and eventually hinder the further IP process. These observations illustrate the inherent self-limiting reaction characteristics of IP process. The existence of abundant unreacted MPD and TMC at each of crosslinking structure further confirms the self-limiting reaction as MPD and TMC cannot contact due to the existence of the crosslinking structure.

It is worthy to not that the reaction is semi-self-limiting because the crosslinking structure does not fully cover the interfacial regions [48]. There is some damage for the penetration of MPD into oil phase as discussed below.

In the end of IP process, all systems exhibited self-limiting behavior irrespective of the molar ratio or the concentration. To gain insights into how the IP reaction proceeds, the formation of chemical bonds during the reaction is then focused on. Given that PA membranes are highly crosslinked, we calculate the evolution of crosslinking degree as the IP reaction progressed. The determination of the crosslinking degree relies on the fraction of the maximum theoretical amide bonds formed [29]. As indicated in Fig. 7, the crosslinking degrees in all cases experienced a rapid increase in the beginning of IP reactions, followed by occasional decreases. Notably, the 10 % concentration cases exhibit a higher increasing rate of crosslinking degrees compared to the 2 % cases. However, once stabilization was reached, the crosslinking degree of the 10 % cases generally fell below that of the 2 % cases. Since the crosslinking process seem distinct for the cases of 2 % concentration with those of 10 %. Such process should be discussed one by one.

3.3.2. *The cases of 2 % concentration*

For the cases of 2 % concentration, there's a relatively lower content of TMC in cases when molar ratio is high. Due to the relatively larger quantity of MPD, these TMC can attract MPD to form a molecular structure of three MPD surrounding TMC. As the molar ratio approaches 3:2, TMC content increases. In this condition, not all TMC are surrounded by three MPD, leaving unreacted acyl-chloride groups in TMC. The more unreacted acyl-chloride groups crosslinking structures have, the lower final degree of crosslinking they exhibit. Therefore, the final degree of crosslinking slightly drops from 0.89 to 0.85 when the molar ratio decreases from 6:1 to 3:2.

Unlike many solvent-free simulation studies, this work involves the free diffusion of monomers in two solvents. This diffusion process undoubtedly affects the final structure of the PA membranes. As discussed above, MPD diffuses slowly than TMC. Experimental setups often employ MPD aqueous solutions with concentrations significantly higher than that of TMC or utilize additives to facilitate the interfacial diffusion of MPD.

When molar ratio become high (6,1), many MPD will penetrate deeper into oil solvent without contacting TMC (shown in Fig. S2a and Fig. S3a). These MPD are often attracted back to the interface due to the accumulation of TMC at the interface (as illustrated in Fig. 5). Such phenomenon results in thinner PA membranes. When molar ratio is reduced to 3:2, indicating the probability of MPD encountering TMC becomes higher and consequently forms oligomers at the position far away from the interface. Since the mobility of oligomers is evidently lower than the one of MPD, the pulling back of oligomers to interface rarely occurs, resulting in the higher density (shown in Fig. 8) at deeper positions in the oil phase. The snail-paced oligomers will further contact with TMC and form the crosslinking structures, resulting in the thicker PA membranes.

As discussed above, the higher molar ratio will result in thinner PA membranes. However, such high molar ration will lead to an excessive accumulation of MPD at the interface, due to the insufficient TMC for crosslinking. It might result in an incomplete PA membrane. In the case of high molar ratio, 6:1, the membrane damage occurs, leading to the drop of ion-rejection performance (shown in Fig. 2a).

3.3.3. *The cases of 10 % concentration*

Due to the higher concentration of MPD (10 %), compared to the case of the same molar ratio, the pulling-back chances of MPD are mainly diminished (shown in Fig. S2c). Moreover, the concentration of TMC is also risen, indicating the large amount of TMC in oil phase and consequently leading to the higher opportunity for MPD to react with TMC (shown in Fig. S3c). Most oligomers can hardly diffuse back to the interfacial region and then crosslinking with each other, leading to a relatively thicker membrane. As shown in Fig. 2b, the thickness of 10 % 6:1 is higher than that of 2 % 6:1 while there is a thicker membrane of 10 % 3:1 compared to the 2 % 3:1 case.

For cases with the same TMC concentration (10 %), a higher molar ratio leads to a reduction in membrane thickness like the cases of 2 % TMC concentration. However, there is an exception, the membrane thickness of 10 % 3:2 case is obviously lower than the other two. The accelerated diffusion caused by excessive concentration of both of two types of monomers leads to a rapid aggregation of monomers at the interface. Consequently, this leads to rapid self-restriction in the interfacial region, isolating the diffusion of monomers and hindering the subsequent self-repair process of the membrane, resulting in a decrease in membrane thickness. The existence of oligomers inside the PA membranes after IP reactions will induce the membrane damage if they cannot combine with crosslinking structures during the post-reaction process, which will be discussed in the coming section. The pronounced damage results in the diminished retention capability, and consequently a notable increase in water flux and a distinct drop in ion rejection.

3.4. *Subsequent treatment process of PA film*

In practical operation, to eliminate residual substances and further enhance the membrane's performance to meet the ultimate utilization objectives, a series of post-treatment steps are usually applied in the experimental method.

Post-reaction of the PA membranes after IP reaction is essential for membrane optimization [49]. Post-reaction curing helps with further crosslinking through additional reactions and increases packing density,

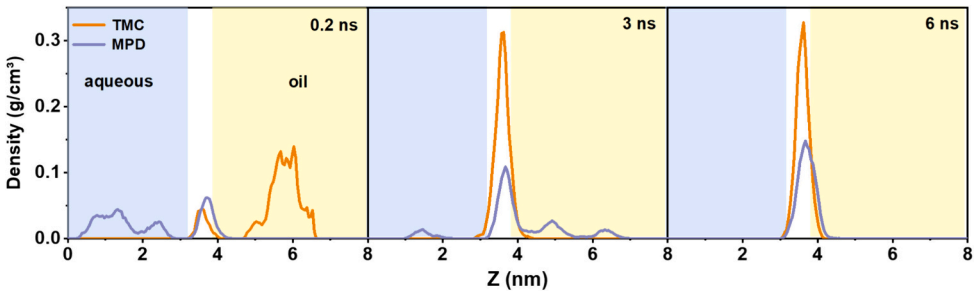

Fig. 5. Density distribution profiles of monomers at distinct simulation time.

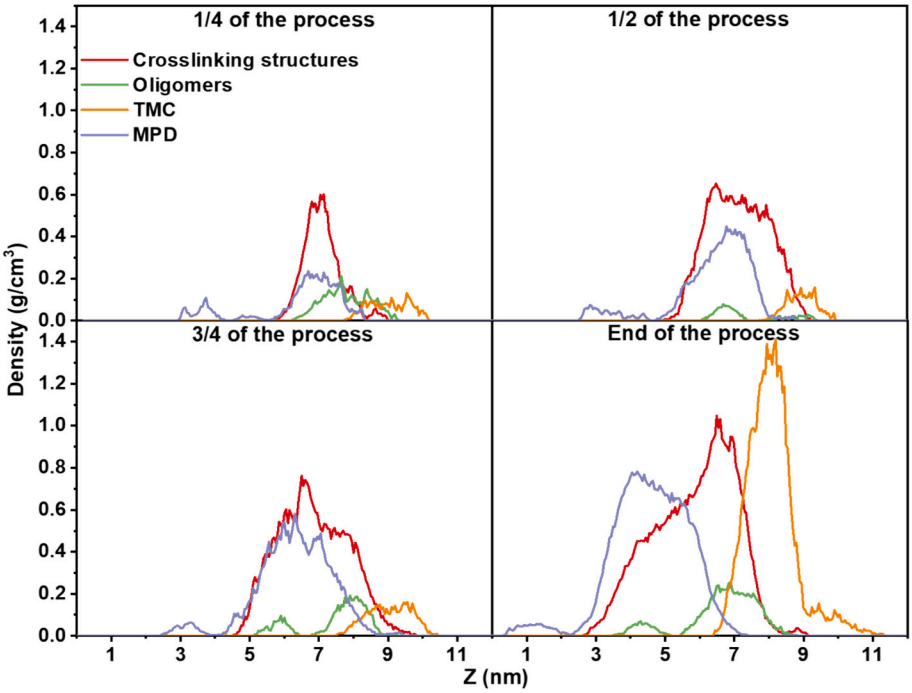

Fig. 6. Density distribution of crosslinking structures, oligomers, TMC and MPD in the case of 2 % 3:2 at various stages of IP process.

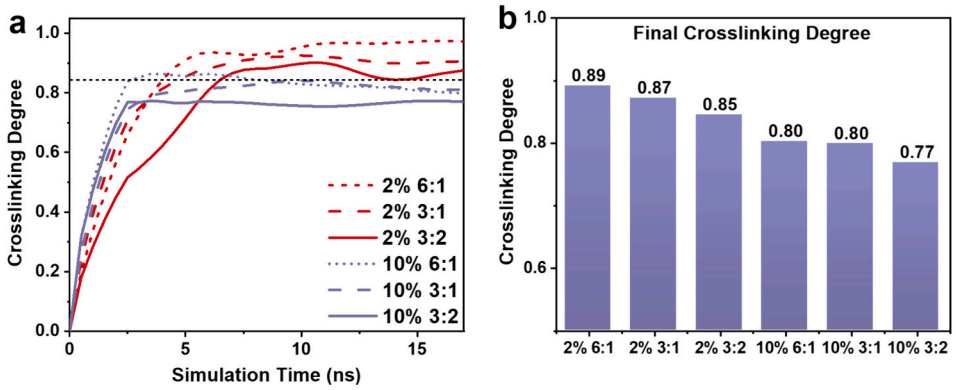

Fig. 7. Crosslinking degree changes over simulation time (a) and the final crosslinking degrees for each case (b).

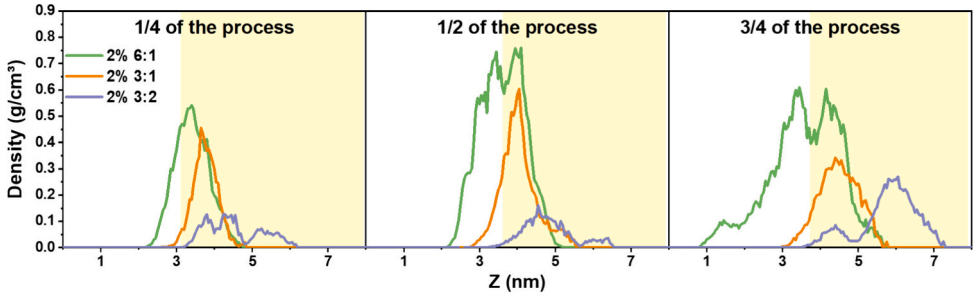

Fig. 8. The density distributions of oligomers in three cases at different stages. For comparison, the edges of the oil phase for three cases are aligned. The oil phase is represented in yellow.

leading to densification of the PA selective layer, which has a significant impact on membrane performance [50]. Numerous studies indicate that curing is a vital factor in stabilizing and enhancing the PA layer. Curing through heat treatment enhances the diffusion rate of the MPD, thereby increasing their availability in the reaction zone and improving the reaction rate. This results in the formation of a thick PA layer, while assisting in shrinking the pores of the substrate membrane, thereby improving the salt rejection [51,52].

During the heat treatment process, the remaining MPD molecules further diffuse into the reaction zone and actively participate in the polymerization process, not the interfacial reaction anymore due to the absence of solvent. The enhanced diffusivity of MPD leads to the further

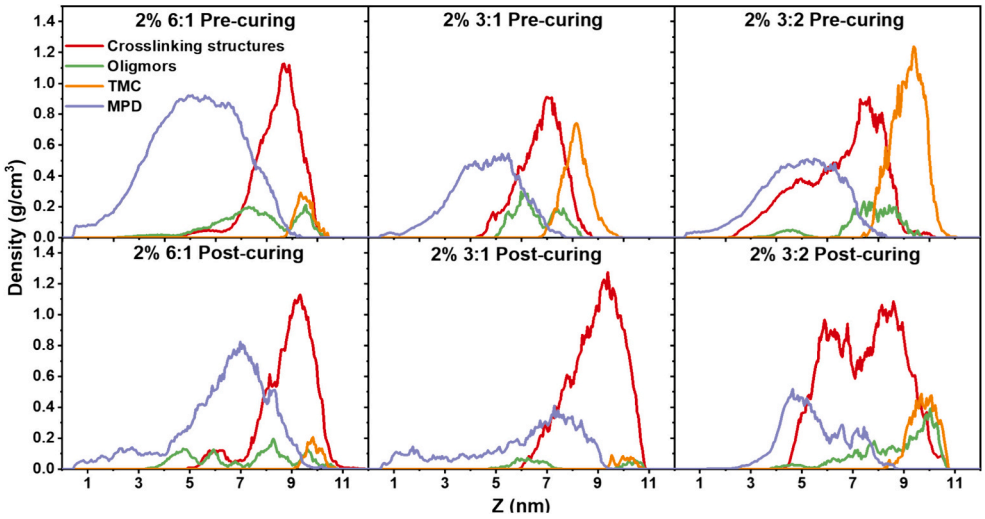

Fig. 9. The density distributions of four various components before and after curing for the cases of 2 % concentration.

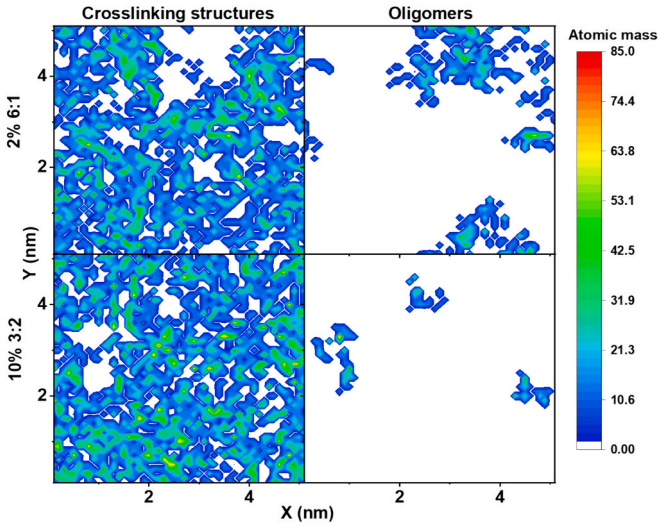

Fig. 10. The atomic mass distribution maps of crosslinking structures (left) and oligomers (right) for two membranes of 2 % 6:1 (upper) and 10 % 3:2 (lower).

crosslinking process. Upon completing the heat treatment, an analysis is conducted by categorizing molecules into four primary components: crosslinking structures, oligomers, TMC and MPD (shown in Fig. 9 and Fig. S4). Prior to heat treatment, a substantial quantity of monomers and oligomers remained attached to the membrane's surface. After heat treatment, there is a notable density reduction of oligomers and monomers, while the density and width of the larger polymer structures increase significantly. This indicates the promotion of crosslinking degrees, which contribute to a further enhancement of membrane densification and an increase in its thickness. The multifaceted impact of heat treatment on the membrane's microstructure and performance is thus underscored.

However, even after heat treatment, 2 % 6:1 and 10 % 3:2 cases still exhibit thinner regions and structural defects. Therefore, the density distribution maps of the two cases are then investigated. As depicted in Fig. 10, the crosslinking structures do not fully cover the entire area, leaving extensive blank spaces. These voids are in accord with the distribution of oligomers, indicating the voids are filled by oligomers.

To further illustrate this phenomenon, VMD snapshots of MD simulations are plotted in Fig. 11. It is observed that both cases have individual oligomers spanning the entire membrane. Since all monomers and oligomers are removed during the washing process (after the curing process), the remained voids cannot be repaired by the final membrane-

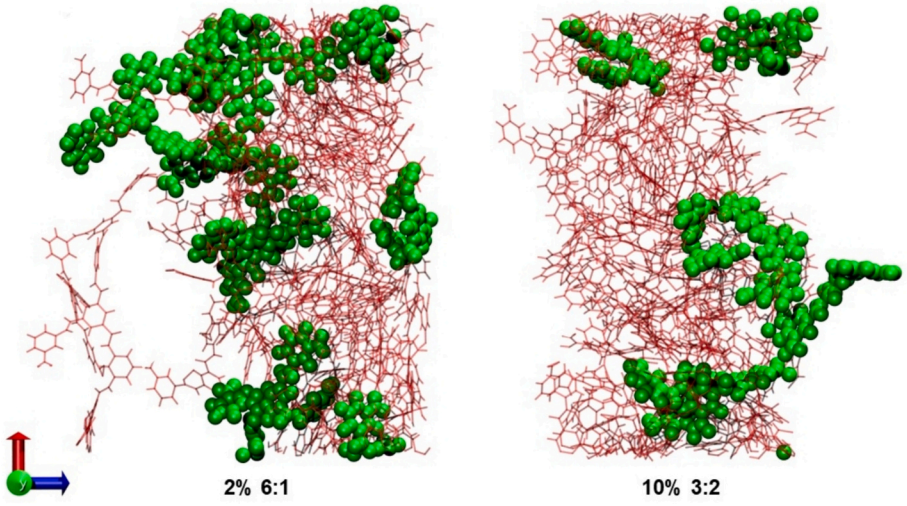

Fig. 11. Snapshots of the two cases, 2 % 6:1, 10 % 3:2. The crosslinking structures are represented in red, and the oligomers are represented in green.

pressing step. In contrast, the other four PA membranes have no oligomers spanning the PA membranes. Moreover, due to their higher membrane thickness, they are better equipped to repair any tiny voids during membrane pressing in NEMD simulations. Hence, these four PA membranes exhibit the fully rejection performance to NaCl (shown in Fig. 2a).

4. Conclusion

This study delves into the dependence of PA-membrane performance on the IP reactions via MD simulations. Thanks to the MD simulations, the details of formation of PA membranes are revealed. For all cases, the self-restricting IP reactions are observed. Once the crosslinking structures, as well as oligomers, form at the interface of two solvents, the penetration of MPD from the aqueous to the oil phase will be hindered. If the crosslinking structures and oligomers occupy the whole interfacial region, the MPD penetrate will stop and the further IP reaction will terminate. As the IP condition changes, e.g. various molar ratio of two types of monomers (MPD and TMC) as well as their initial concentrations in solvents (water and n-hexane, respectively), the obtained PA membranes have distinct molecular structures with various thickness, porosities and specific surface areas, and consequently exhibit various permeance and rejection performance. When large molar ratio, e.g. MPD/TMC = 6:1, is applied, the MPD firstly penetrate deep into the oil phase because of the large concentration gradient, but rarely contact with TMC for IP reaction because of the relatively fewer TMC in the oil phase. Those MPD will be pulled back to the interface for the IP reaction. Such pulling back process will result in a thinner PA membrane (1.7 nm), which has promoted permeance (51.16 LMHB). However, the extremely thin PA membrane will occasionally lead to the membrane damage, which will of course reduce the NaCl-rejection performance. When the molar ratio is as low as 3:2, the mobile MPD will react with TMC to form oligomers deep within the oil phase, and the snail-paced oligomers will further react with MPD and TMC to form crosslinking structure at the position deep within the oil phase. This consequently results in the thicker PA membranes with lower permeance (9.38 LMHB). The higher concentrations of both types of monomers will certainly raise the contact and reaction opportunity of TMC and MPD in the oil phase, resulting in a thicker PA membrane. However, the existence of spanning oligomers in PA membranes should be focused on because they will induce the membrane damage during the rinsing process. In this study, we provide a thorough understanding of the crucial diffusion and reaction steps involved in the preparation of PA membranes. By fine-tuning performance at the microscopic level, effective optimization of membrane flux and structure can be achieved. This offers valuable insights into the design and fabrication of high-performance PA membranes. Furthermore, the method applied in this work can be extended to the investigation of the impact of temperature, support, etc., on the formation of PA membranes. Once these findings are confirmed by the experiments, this offers valuable insights into the design and fabrication of high-performance PA membranes.

Declaration of competing interest

The authors declare that they have no known competing financial interests or personal relationships that could have appeared to influence the work reported in this paper.

Data availability

Data will be made available on request.

Acknowledgement

This work was financially supported by the National Natural Science Foundation of China (21921006, 22278206) and the Key Research and Development Program of Jiangsu Province (BE2021714). The authors also thank the High Performance Computing Centre of Nanjing Tech University for supporting the computational resources.

Appendix A. Supplementary data

Supplementary data to this article can be found online at https://doi.org/10.1016/j.desal.2024.117869.

References

[1] E. Jones, M. Qadir, M.T.H. van Vliet, V. Smakhtin, S.M. Kang, The state of desalination and brine production: a global outlook, Sci. Total Environ. 657 (2019) 1343–1356, https://doi.org/10.1016/j.scitotenv.2018.12.076.
[2] A. Yusuf, A. Sodiq, A. Giwa, J. Eke, O. Pikuda, G. De Luca, J.L. Di Salvo, S. Chakraborty, A review of emerging trends in membrane science and technology for sustainable water treatment, J. Clean. Prod. 266 (2020), https://doi.org/10.1016/j.jclepro.2020.121867.
[3] M.Q. Seah, W.J. Lau, P.S. Goh, H.H. Tseng, R.A. Wahab, A.F. Ismail, Progress of interfacial polymerization techniques for polyamide thin film (Nano)composite membrane fabrication: a comprehensive review, Polymers 12 (12) (2020), https://doi.org/10.3390/polym12122817.
[4] Z. Yang, Y. Zhou, Z. Feng, X. Rui, T. Zhang, Z. Zhang, A Review on Reverse Osmosis and Nanofiltration Membranes for Water Purification, Polymers 11 (8) (2019), https://doi.org/10.3390/polym11081252.
[5] J.R. Werber, A. Deshmukh, M. Elimelech, The critical need for increased selectivity, not increased water permeability, for desalination membranes, Environ. Sci. Technol. Lett. 3 (4) (2016) 112–120, https://doi.org/10.1021/acs.estlett.6b00050.
[6] Q.-W. Meng, L. Cheng, Q. Ge, Recent advances and future challenges of polyamide-based chlorine-resistant membrane, Advanced Membranes 3 (2023) 100075, https://doi.org/10.1016/j.advmem.2023.100075.
[7] Z. Wang, X. Luo, J. Zhang, F. Zhang, W. Fang, J. Jin, Polymer membranes for organic solvent nanofiltration: recent progress, challenges and perspectives, Advanced Membranes 3 (2023) 100063, https://doi.org/10.1016/j.advmem.2023.100063.
[8] J.L. He, T. Arbaugh, D. Nguyen, W.K. Xian, E.M.V. Hoek, J.R. McCutcheon, Y. Li, Molecular mechanisms of thickness-dependent water desalination in polyamide reverse-osmosis membranes, J. Membr. Sci. 674 (2023), https://doi.org/10.1016/j.memsci.2023.121498.
[9] W. Zhang, R. Chu, W. Shi, Y. Hu, Quantitively unveiling the activity-structure relationship of polyamide membrane: a molecular dynamics simulation study, Desalination 528 (2022), https://doi.org/10.1016/j.desal.2022.115640.
[10] W. Zhang, Y. Qin, W. Shi, Y. Hu, Unveiling the molecular mechanisms of thickness-dependent water dynamics in an ultrathin free-standing polyamide membrane, J. Phys. Chem. B 124 (52) (2020) 11939–11948, https://doi.org/10.1021/acs.jpcb.0c07263.
[11] N. Akther, Y. Kawabata, S. Lim, T. Yoshioka, S. Phuntsho, H. Matsuyama, H. K. Shon, Effect of graphene oxide quantum dots on the interfacial polymerization of a thin-film nanocomposite forward osmosis membrane: an experimental and molecular dynamics study, J. Membr. Sci. 630 (2021), https://doi.org/10.1016/j.memsci.2021.119309.
[12] D.W. Ma, Z. Zhang, S. Xiong, J.M. Zhou, Y. Wang, Additive manufacturing of defect-healing polyamide membranes for fast and robust desalination, J. Membr. Sci. 671 (2023) 8, https://doi.org/10.1016/j.memsci.2023.121407.
[13] P. Hu, B.B. Yuan, Q.J. Niu, K. Chen, Z.W. Xu, B.Z. Tian, X.Z. Zhang, Modification of polyamide nanofiltration membrane with ultra-high multivalent cations rejections and mono−/divalent cation selectivity, Desalination 527 (2022), https://doi.org/10.1016/j.desal.2022.115553.
[14] M. Ding, A. Szymczyk, A. Ghoufi, Hydration of a polyamide reverse-osmosis membrane, J. Membr. Sci. 501 (2016) 248–253, https://doi.org/10.1016/j.memsci.2015.12.036.
[15] T. Wei, L. Zhang, H. Zhao, H. Ma, M.S. Sajib, H. Jiang, S. Murad, Aromatic polyamide reverse-osmosis membrane: an atomistic molecular dynamics simulation, J. Phys. Chem. B 120 (39) (2016) 10311–10318, https://doi.org/10.1021/acs.jpcb.6b06560.
[16] L. Wang, R.S. Dumont, J.M. Dickson, Molecular dynamic simulations of pressure-driven water transport through polyamide nanofiltration membranes at different membrane densities, RSC Adv. 6 (68) (2016) 63586–63596, https://doi.org/10.1039/c6ra12115b.
[17] J. He, J.R. McCutcheon, Y. Li, Effect of different manufacturing methods on polyamide reverse-osmosis membranes for desalination: insights from molecular dynamics simulations, Desalination 547 (2023), https://doi.org/10.1016/j.desal.2022.116204.
[18] Y. Song, M.J. Wei, F. Xu, Y. Wang, Molecular simulations of water transport resistance in polyamide RO membranes: interfacial and interior contributions, Engineering-Prc 6 (5) (2020) 577–584, https://doi.org/10.1016/j.eng.2020.03.008.
[19] Y. Song, M.J. Wei, F. Xu, Y. Wang, Transport mechanism of water molecules passing through polyamide/COF mixed matrix membranes, Phys. Chem. Chem. Phys. 21 (48) (2019) 26591–26597, https://doi.org/10.1039/c9cp05026d.
[20] W. Huang, Z. Wang, F. Xie, H. Ding, W. Li, X. Liang, X. Ma, Z. Xu, High performance polyamide TFC reverse osmosis membrane fabricated on co-

deposition hydrophilic modified polyethylene substrate, Desalination 538 (2022), https://doi.org/10.1016/j.desal.2022.115909.
[21] Q. Li, K. Zhao, Q. Liu, J. Wang, Desalination behavior analysis of interior-modified carbon nanotubes doped membrane by dielectric spectrum and molecular simulation, Nanotechnology 31 (31) (2020) 315705, https://doi.org/10.1088/1361-6528/ab8988.
[22] G. Wang, X. Zhang, M. Wei, Y. Wang, Mechanism of permeance enhancement in mixed-matrix reverse osmosis membranes incorporated with graphene and its oxides, Sep. Purif. Technol. 270 (2021), https://doi.org/10.1016/j.seppur.2021.118818.
[23] Y. Song, F. Xu, M.J. Wei, Y. Wang, Water flow inside Polamide reverse osmosis membranes: a non equilibrium molecular dynamics study, J. Phys. Chem. B 121 (7) (2017) 1715–1722, https://doi.org/10.1021/acs.jpcb.6b11536.
[24] Q.A. Gu, L. Liu, Y. Wang, C. Yu, Surface modification of polyamide reverse osmosis membranes with small-molecule zwitterions for enhanced fouling resistance: a molecular simulation study, Phys. Chem. Chem. Phys. 23 (11) (2021) 6623–6631, https://doi.org/10.1039/d0cp06383e.
[25] M.S. Jahan Sajib, Y. Wei, A. Mishra, L. Zhang, K.I. Nomura, R.K. Kalia, P. Vashishta, A. Nakano, S. Murad, T. Wei, Atomistic simulations of biofouling and molecular transfer of a cross-linked aromatic polyamide membrane for desalination, Langmuir 36 (26) (2020) 7658–7668, https://doi.org/10.1021/acs.langmuir.0c01308.
[26] M. Ding, A. Ghoufi, A. Szymczyk, Molecular simulations of polyamide reverse osmosis membranes, Desalination 343 (2014) 48–53, https://doi.org/10.1016/j.desal.2013.09.024.
[27] Y. Luo, E. Harder, R.S. Faibish, B. Roux, Computer simulations of water flux and salt permeability of the reverse osmosis FT-30 aromatic polyamide membrane, J. Membr. Sci. 384 (1–2) (2011) 1–9, https://doi.org/10.1016/j.memsci.2011.08.057.
[28] V. Kolev, V. Freger, Hydration, porosity and water dynamics in the polyamide layer of reverse osmosis membranes: a molecular dynamics study, Polymer 55 (6) (2014) 1420–1426, https://doi.org/10.1016/j.polymer.2013.12.045.
[29] R. Vickers, T.M. Weigand, C.T. Miller, O. Coronell, Molecular methods for assessing the morphology, topology, and performance of polyamide membranes, J. Membr. Sci. 644 (2022), https://doi.org/10.1016/j.memsci.2021.120110.
[30] L. Shen, R.H. Cheng, M. Yi, W.S. Hung, S. Japip, L. Tian, X. Zhang, S.D. Jiang, S. Li, Y. Wang, Polyamide-based membranes with structural homogeneity for ultrafast molecular sieving, Nat. Commun. 13 (1) (2022), https://doi.org/10.1038/s41467-022-28183-1.
[31] M.R. Chowdhury, J. Steffes, B.D. Huey, J.R. McCutcheon, 3D printed polyamide membranes for desalination, Science 361 (6403) (2018) 682–685, https://doi.org/10.1126/science.aar2122.
[32] C. Liu, J. Yang, B.B. Guo, S. Agarwal, A. Greiner, Z.K. Xu, Interfacial polymerization at the alkane/ionic liquid interface, Angew. Chem. Int. Ed. 60 (26) (2021) 14636–14643, https://doi.org/10.1002/anie.202103555.
[33] W.D. Mulhearn, V.P. Oleshko, C.M. Stafford, Thickness-dependent permeance of molecular layer-by-layer polyamide membranes, J. Membr. Sci. 618 (2021), https://doi.org/10.1016/j.memsci.2020.118637.
[34] S. Qiu, L. Wu, L. Zhang, H. Chen, C. Gao, Preparation of reverse osmosis composite membrane with high flux by interfacial polymerization of MPD and TMC, J. Appl. Polym. Sci. 112 (4) (2009) 2066–2072, https://doi.org/10.1002/app.29639.
[35] N. Zhang, S. Chen, B. Yang, J. Huo, X. Zhang, J. Bao, X. Ruan, G. He, Effect of hydrogen-bonding interaction on the arrangement and dynamics of water confined in a polyamide membrane: a molecular dynamics simulation, J. Phys. Chem. B 122 (17) (2018) 4719–4728, https://doi.org/10.1021/acs.jpcb.7b12790.
[36] A.I. Jewett, D. Stelter, J. Lambert, S.M. Saladi, O.M. Roscioni, M. Ricci, L. Autin, M. Maritan, S.M. Bashusqeh, T. Keyes, R.T. Dame, J.E. Shea, G.J. Jensen, D. S. Goodsell, Moltemplate: a tool for coarse-grained modeling of complex biological matter and soft condensed matter physics, J. Mol. Biol. 433 (11) (2021), https://doi.org/10.1016/j.jmb.2021.166841.
[37] H. Zhang, M.S. Wu, K. Zhou, A.W.K. Law, Molecular insights into the composition-structure-property relationships of polyamide thin films for reverse osmosis desalination, Environ. Sci. Technol. 53 (11) (2019) 6374–6382, https://doi.org/10.1021/acs.est.9b02214.
[38] L.J. Abbott, K.E. Hart, C.M. Colina, Polymatic: a generalized simulated polymerization algorithm for amorphous polymers, Theor. Chem. Accounts 132 (3) (2013) 1334, https://doi.org/10.1007/s00214-013-1334-z.
[39] C. Jang, T.W. Sirk, J.W. Andzelm, C.F. Abrams, Comparison of crosslinking algorithms in molecular dynamics simulation of thermosetting polymers, Macromol. Theory Simul. 24 (3) (2015) 260–270, https://doi.org/10.1002/mats.201400094.
[40] S. Plimpton, Fast parallel algorithms for short-range molecular-dynamics, J. Comput. Phys. 117 (1) (1995) 1–19, https://doi.org/10.1006/jcph.1995.1039.
[41] J. Wang, R.M. Wolf, J.W. Caldwell, P.A. Kollman, D.A. Case, Development and testing of a general amber force field, J. Comput. Chem. 25 (9) (2004) 1157–1174, https://doi.org/10.1002/jcc.20035.
[42] S.P. Kadaoluwa Pathirannahalage, N. Meftahi, A. Elbourne, A.C.G. Weiss, C. F. McConville, A. Padua, D.A. Winkler, M. Costa Gomes, T.L. Greaves, T.C. Le, Q. A. Besford, A.J. Christofferson, Systematic comparison of the structural and dynamic properties of commonly used water models for molecular dynamics simulations, J. Chem. Inf. Model. 61 (9) (2021) 4521–4536, https://doi.org/10.1021/acs.jcim.1c00794.
[43] M. Shen, S. Keten, R.M. Lueptow, Rejection mechanisms for contaminants in polyamide reverse osmosis membranes, J. Membr. Sci. 509 (2016) 36–47, https://doi.org/10.1016/j.memsci.2016.02.043.
[44] X. Zhang, M.J. Wei, F. Xu, Y. Wang, Thickness-dependent ion rejection in nanopores, J. Membr. Sci. 601 (2020), https://doi.org/10.1016/j.memsci.2020.117899.
[45] T.E. Culp, B. Khara, K.P. Brickey, M. Geitner, T.J. Zimudzi, J.D. Wilbur, S.D. Jons, A. Roy, M. Paul, B. Ganapathysubramanian, A.L. Zydney, M. Kumar, E.D. Gomez, Nanoscale control of internal inhomogeneity enhances water transport in desalination membranes, Science 371 (6524) (2021) 72–75, https://doi.org/10.1126/science.abb8518.
[46] J.R. McCutcheon, Unraveling the mysteries of the thin film composite reverse osmosis membrane, Joule 5 (3) (2021) 528–530, https://doi.org/10.1016/j.joule.2021.03.004.
[47] S. Karan, Z. Jiang, A.G. Livingston, Sub-10 nm polyamide nanofilms with ultrafast solvent transport for molecular separation, Science 348 (6241) (2015) 1347–1351, https://doi.org/10.1126/science.aaa5058.
[48] K. Grzebyk, M.D.D. Armstrong, O. Coronell, Accessing greater thickness and new morphology features in polyamide active layers of thin-film composite membranes by reducing restrictions in amine monomer supply, J. Membr. Sci. 644 (2022), https://doi.org/10.1016/j.memsci.2021.120112.
[49] T.A. Otitoju, R.A. Saari, A.L. Ahmad, Progress in the modification of reverse osmosis (RO) membranes for enhanced performance, J. Ind. Eng. Chem. 67 (2018) 52–71, https://doi.org/10.1016/j.jiec.2018.07.010.
[50] M. Zargar, B. Jin, S. Dai, An integrated statistic and systematic approach to study correlation of synthesis condition and desalination performance of thin film composite membranes, Desalination 394 (2016) 138–147, https://doi.org/10.1016/j.desal.2016.05.014.
[51] S. Habib, S.T. Weinman, A review on the synthesis of fully aromatic polyamide reverse osmosis membranes, Desalination 502 (2021), https://doi.org/10.1016/j.desal.2021.114939.
[52] B. Khorshidi, T. Thundat, B.A. Fleck, M. Sadrzadeh, A novel approach toward fabrication of high performance thin film composite polyamide membranes, Sci. Rep.-Uk 6 (2016), https://doi.org/10.1038/srep22069.